2024 IEEE/RSJ International Conference on Intelligent Robots and Systems (IROS)
October 14-18, 2024. Abu Dhabi, UAE

A Novel Vitreoretinal Surgical Robot System to Maximize the Internal Reachable Workspace and Minimize the External Link Motion*

Gowoon Jeong and Seong Yeong Ko, *Member, IEEE*

***Abstract*—This paper presents a novel robotic system designed for efficient minimally invasive eye surgery. The proposed prototype integrates a concentric tube mechanism(CTM) and a belt-driven remote center of motion(RCM) mechanism, aiming to maximize the internal reachable workspace while minimizing external robot movements. The integrated system provides several advantages, including preventing collisions between surgical tools and the lens, minimizing sclera stress, and having efficient robot motion inside and outside the eyeball. It provides sufficient link motions with roll and pitch angles of ±32° and ±85° respectively at the RCM point, allowing access to 89% of the retina. The experiment evaluates the system's performance, with the RCM point accuracy at 0.718mm, CTM position accuracy at 207 µm, and a repeatability error of 246 µm. To reduce hysteresis errors at the RCM point caused by the belt, a lever-based belt tensioner is used for initial calibration while an optical tracking system tracks each joint's movement. Targeting experiments highlight that the wider workspace was achieved by the CTM+RCM system compared to the traditional RCM mechanism with a straight tool. The results showed the system's compactness, efficiency, and dexterity, confirming its feasibility and potential for the proposed eye surgery robot.**

I. Introduction

Vitreoretinal surgery is a minimally invasive surgery that requires the surgeon's precise movements and skilled dexterity. A surgeon inserts the straight rigid instrument through the small incision hole about 4 mm away from the cornea limbus and the tool reaches to retina [1]. The surgeon needs to perform micro-scale surgical tasks such as epiretinal membrane peeling, retinal vein cannulation, and subretinal injection [2]. However, the physiological hand tremors may cause positioning errors of the tool tip, which can cause patient tissue damage and bleeding [3].

Robotic systems have steadily improved the performance of safe minimally invasive eye surgery for almost three decades [4]. A limited surgical environment is imposed, including anatomical constraints inside the eyeball and the installation of a microscope or other instruments outside the eyeball. So, surgical robots aim to develop systems that can effectively perform surgical tasks both inside and outside the eyeball.

In the case of using conventional long and slender tools, there can be the risk of colliding with the lens when the tools need to reach the outer portion of the retina, and the limitation of flexibility due to their rigid structure makes it difficult to meet precise surgical accuracy requirements [5]. Additionally, the large tilting motion of the tools can cause large scleral stress along with scarring around the insertion point [6,7]. To deal with these problems, researchers have tried to develop dexterous instruments to provide an additional degree of freedom (DOF) at the distal part. The tool tip is bent or is made to be steerable considering the approaching angle between the surgical tip and the retinal tissue. These instruments include bendable forceps [8], a stent deployment unit [9], and a variable neutral-line snake-type mechanism [10]. A concentric tube robot (CTR) has been widely investigated these days for use in surgical procedures due to its dexterous nature and ease of miniaturization [11]. Lin et al. proposed the CTR-based eye surgery robot, which showed that the use of CTR could reduce stress near the insertion point and increase the workspace compared to using a straight tool alone by considering the anatomy of the eyeball [6].

In early work, our research group proposed a force-sensing concentric tube-based vitreoretinal surgical robot [12]. However, despite having many advantages, CTR alone still has problems for use as a medical robot. For example, the overall curvature of the robot depends on the relative length of the tube and requires optimization for trajectory planning due to the curvature limitation. Moreover, the high DOF system may cause issues such as the complexity of modeling, computational costs, and a larger number of actuators [13]. To solve this issue, we proposed a robotic system that integrates the CTR and the external motion mechanism, but the external motion robot is mainly used to complement the CTR. For similar reasons, Johns Hopkins University researchers developed the Steady-Hand Eye Robot (SHER) [14], and integrated the snake-like bendable needle system called IRIS [10] and I2RIS [15] to complement its dexterity. The movements inside and outside the eyeball are designed to have a complementary relationship, so we considered integrating CTR with the external motion mechanism.

Since vitreoretinal surgery is a minimally invasive surgery, a trocar point is made for tool insertion in the cornea to reduce eye damage. In addition, in a surgical environment with microscopes and other tools, the placement of a robot system has spatial constraints as well. The remote center of motion (RCM) mechanism is well-suited for eye surgery due to its

*This paper was supported by the National Research Foundation of Korea (NRF) grant funded by the Korean government (MSIT) (No.2022R1A2C2008422).

G. Jeong is with the Department of Mechanical Engineering, Graduate School, Chonnam National University, Gwangju, 61186, Republic of Korea (e-mail: gjeong@jnu.ac.kr).

S. Y. Ko is with the School of Mechanical Engineering, Chonnam National University, Gwangju, 61186, Republic of Korea (corresponding author phone number: +82-62-530-1679; fax: +82-62-530-1689; e-mail: sko@jnu.ac.kr).

unique feature of having a fixed point (RCM) that acts as a center of rotation of the mechanism, even in the absence of a physical joint at that point. The double-parallelogram RCM mechanism is the most well-known design topology, with several researchers developing the surgical robot using this structure [16-18]. The 5-DOF Ophthalmic Micrography Robot (OmSR) system [19] and the arc-type RCM mechanisms [20] for retinal surgery have been developed and verified their usefulness. Although mechanisms such as double-parallelogram structures are widely used because they provide precise motion, they have the problem of exposing a large number of links and passive joints to the outside. Additionally, the external link's movements need to be minimized as much as possible to reduce the scleral stress associated with the RCM mechanism and prevent interference with surgeons or other surgical tools.

In this paper, we introduce a novel vitreoretinal surgery robot integrating a miniaturized CTM module for internal motion and a belt-driven RCM mechanism for external motion. The integration of the 4-DOF CTM and the 2-DOF RCM mechanism offers several advantages, such as preventing tool collisions on the lens, reducing scleral stress, additional hardware stability, and safety motions along the physically constrained pivot point. We designed a compact and practical robot that considers the eye surgery environment, which features efficient movement inside and outside the eye and a large workspace for the retina. The rest of this paper is organized as follows. The following sections introduce the design of the mechanism in Chapter II, and the analysis of the integrated mechanism in Chapter III. The experiment to evaluate the built robot is provided in Chapter IV and conclusions and future work are discussed in Chapter V.

II. Mechanism Design of Proposed Eye Surgery Robot

A. Minimized Concentric Tube Mechanism Design

The concentric tube mechanism (CTM) consists of pre-curved and super-elastic tubes nested inside of each other and the shape of the integrated tube is a function of relative translational and rotational movement of the inner and outer tubes [21]. When designing an actuating system for a 4-DOF CTM with two tubes, constraints related to eye surgeries were carefully considered. The robot's target is the retina, which covers two-thirds of the endometrium, and the lens is considered as an obstacle. The average diameter of the eye $D_{avg.eye}$ is about 24 mm, but the maximum distance between different regions of the retina is 25.8 mm [22].

The actuator stroke $L_{Actuator}$ needs to satisfy the condition $L_{Actuator} > L_{safe} + D_{avg.eye}$, where L_{safe} denotes a safety factor that prevents the robot from colliding with the eyeball and we chose L_{safe} =30 mm in our work. Additionally, given that tools used in eye surgery typically range from 25 to 20 gauge [23], we decided the outer tube's maximum diameter to be less than 22 gauge. Considering the integration of a fiber Bragg grating (FBG) sensor and/or a gripper inside the inner tube in the future as mentioned in [24], we followed the design method considering stiffness ratio as shown in Fig.1 and Table. I. This ensures compatibility with the dimensions of tools commonly employed in eye surgery procedures.

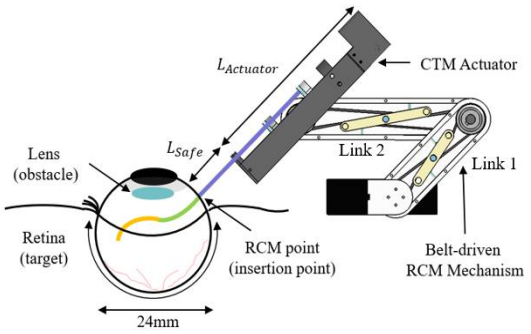

Figure 1. Concept of mechanism and design considerations.

We designed the miniaturized actuating module for CTM which has two moving slides for each tube. Hendrick et al. proposed a robotic system for transurethral laser prostate surgery [24] and it has the potential to be miniaturized. As shown in Fig. 2, four DC motors (Maxon co., RE8) are used for the miniaturized actuator. Two motors produce the translation motion of the tubes via lead screws and nuts, and the remaining two motors transmit the rotation motion through a square bar and the gear mechanism with a square hole in the gear. Bearings are integrated into both the sliding and fixed components of all rotating parts. The mechanical components of each slide are selected to minimize the size while ensuring smooth gear rotation during slide movement.

The developed actuator module was fabricated to be compact, with an overall size of 27 mm × 161 mm × 31.5 mm (width × length × height), as shown in Fig. 2. This is a significant size reduction compared to other CTM actuators used for eye surgery [12, 24] or in other applications [25]. It is also comparable to the smallest actuator designed for eye surgery [6].

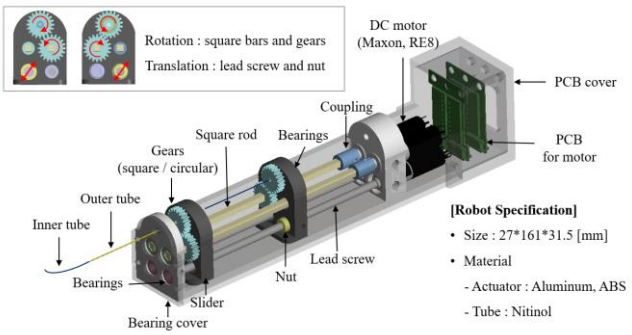

Figure 2. 3D model of the miniaturized CTM module

TABLE I. Details of Each Concentric Tube

	Outer tube		*Inner tube*	
	Symbol	**Dimension**	**Symbol**	***Dimension***
Outer diameter	OD_1	0.635mm	OD_2	0.4 mm
Inner diameter	ID_1	0.48mm	ID_2	0.2 mm
Radius of curvature	r_1	24 mm	r_2	27 mm
Curved part length	$l_{1,1}$	14.5 mm	$l_{2,1}$	15 mm
Straight part length	$l_{1,2}$	37 mm	$l_{2,2}$	57 mm

B. Timming Belt-Driven RCM mechanism Design

A belt-driven RCM mechanism was chosen for the external movement of the CTM module. The mechanism is known to be compact and has the advantage of hiding the complex structure inside since it transmits the power using a belt and can maintain a parallelogram configuration with only two serially connected links [25]. To design the compact 2-DOF RCM mechanism for eye surgery, its compactness, compatibility with the CTM, and RCM point positioning alignment with the insertion point on the sclera are mainly considered. The mechanism, utilizing two timing belts and four timing pulleys, facilitates size reduction while ensuring precise control without slipping.

Fig. 3 illustrates how two-timing belts drive two links, maintaining a parallelogram configuration for *x*-axis rotation at a fixed RCM point. The other motor rotates the entire CTM-integrated system along the y-axis. A lever-based tensioner was chosen for its simultaneous tensioning ability, providing high resolution through adjustable screw pitch. The length of links of the RCM mechanism was selected to tilt outward from the patient's head, ensuring unobstructed access to the retina without interfering with the microscope.

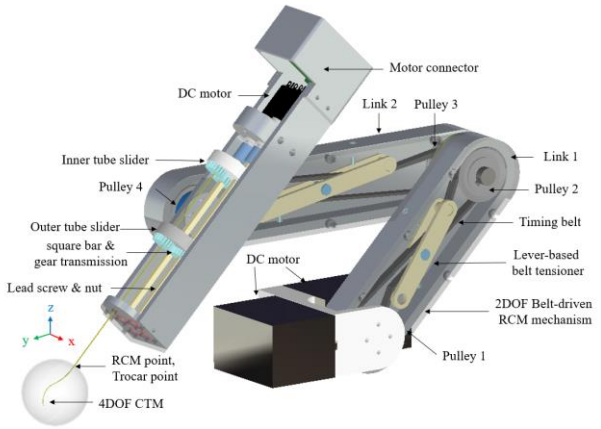

Figure 3. Prototype incorporating CTM and RCM mechanism.

The robotic system for vitreoretinal surgery needs to provide sufficient tilting angles, with roll and pitch within the range of ±30°, and yaw extending to 360° [26]. In the case of using a straight tool, the maximum tilting angles reported are 60° for roll and 90° for pitch [27]. The robot's link lengths were designed to accommodate not only the CTM but also the straight tools, enabling versatility in robot operation.

As depicted in Fig. 1, the actuator length of CTM was set to L_{CTM} = 140 mm, and the lengths of Link 1 and Link 2 are chosen as L_1 = 90 mm and L_2 = 140 mm, respectively. The additional initial tilting angle to compensate for the tool offset is determined considering the geometric constraints and was determined to be θ_{int} = 10.2° in this work. The system allows the pivoting motion of ±32° for roll motion and ±85° for pitch motion. This confirms its capability to satisfy the required workspace and not collide with the patient as shown in Fig. 4. To minimize the effect of gear backlash, a combination of the EC motor (Maxon Motor Co., EC 32 flat) and a harmonic drive (Samick HDS co., CSF-8B-100-2XH-F, gear ratio 100:1) combination is used.

C. Manufactured prototype

The main frames of the CTM and RCM mechanism were machined from aluminum, while sliders, small gears, couplings, and square bars were fabricated using 3D printing techniques with ABS material. The concentric tubes were made from nitinol tubes and pre-bent utilizing the shape memory alloy properties. The tubes were heated in a furnace at a rate of 10°C/min to 550°C and held at that temperature for 30 minutes before quenching in cold water [12]. The curvature of each tube was fixed using metal plates with radii of curvature measuring 27mm and 24mm, respectively. The fabricated needles were attached to the driving gear components using instant glue.

Figure 4. Manufactured prototype considering the surgical environment

III. Mechanism Incorporating CTM and RCM

A. Workspace Analysis

The workspace required for retinal surgery is restricted to the microscope view. However, surgeons can access a wider workspace (a wider portion of the retina) by rotating the eyeball. To analyze the workspace for retinal surgery, we obtained three-dimensional spherical reachable workspaces on the retina in three cases: RCM + straight tool, CTM only, and CTM+RCM.

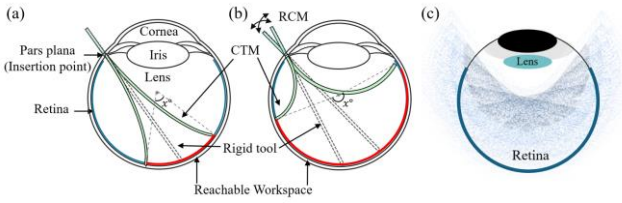

Figure 5. Workspace Analysis

The CTM exhibits a conical workspace when modeled using a torsionally compliant model [24]. The angle $x°$ on a plane as shown in Fig. 5(a) and 5(b), representing the arc around the eyeball's center, is twice the tilting angle of the robot. The intersection of the robot's workspace and the retina forms a spherical cap. To calculate the robot's workspace S_x with a spherical curvature matching the eye radius r, equation (1) is derived using volume integration.

$$S_x = 2\pi \int_{r\cos\left(\frac{x°}{2}\right)}^{r} r\,dx = 2\pi r^2\left(1-\cos\left(\frac{x°}{2}\right)\right) \quad (1)$$

Since the retina corresponds to x=240°, (2) allows us to determine the extent to which the surgical tool tip can reach the retina in terms of the angle $x°$.

$$\frac{S_x}{S_{retina}} = \frac{2\pi r^2\left(1-\cos\left(\frac{x}{2}\right)\right)}{2\pi r^2\left(1-\cos\left(\frac{240°}{2}\right)\right)} = \frac{2}{3}\left(1-\cos\left(\frac{x}{2}\right)\right)\times 100\% \quad (2)$$

Our study integrated the RCM mechanism into the CTM to expand the workspace, ensuring safe navigation around the lens and reaching the retina from the insertion point. The workspace analysis, using the parameters in Table 1, was conducted in MATLAB software. Based on analysis results as shown in Fig. 5(c), the 30° tilting motion along the x-axis shows a significant expansion to the whole workspace. In addition, when a 30° tilting motion along the y-axis is also combined, sufficient workspace for the retinal surgery could be obtained.

C. Kinematics of Integrated System

A torsionally compliant model based on the Cosserat rod theory was utilized for CTM modeling [21]. This simplified model, though not comprehensive in accounting for all physical parameters, seems suitable for its computational efficiency despite some inherent inaccuracies. Using the forward kinematics f, where the input is motor values q=[l_1, α_1, l_r, α_r]^T and the output is X=[x, y, z, t_x, t_y, t_z]^T [28], the inverse kinematics can be obtained by deriving the Jacobian matrix J as provided in [29], and then by using the Newton-Raphson method to calculate the joint values using the equation $q^{k+1} = q^k - J^+(q^k)[f(q^k) - f(q^{des})]$, where k, J^+, and q^{des} denote an iteration number, a pseudo-inverse Jacobian matrix, and the desired joint value to reach the target in Cartesian space. The kinematics of the RCM mechanism is simpler, with the tilting angles in the x and y axes matching the motor inputs, allowing for a cost-effective computation as shown in (3).

$$q_{Rx} = \theta_{RCM,x},\ q_{Ry} = \theta_{RCM,y} + \theta_{init} \quad (3)$$

where, q_{Rx} and q_{Ry} denote the motors' tilting angles of the RCM mechanism along x-axis and y-axis, respectively, and $\theta_{RCM,x}$ and $\theta_{RCM,y}$ denote the tool's tilting angles at the RCM point along x-axis and y-axis, respectively. We implemented a teleoperating system using this kinematics. The 3D system's Omni Touch haptic device was used as the remote controller running in an Ubuntu 20.04 LTS environment integrated with ROS Noetic. Open Haptics and the Phantom Omni open source [30] were utilized in the integration process.

IV. Experiment

A. Initial Calibration for RCM mechanism

The belt-driven RCM mechanism requires initial calibration. We manually calibrated it using belt tensioners. To track the movement of each joint, we attached an infra-red (IR) marker to each joint and tracked the path and the angles of joints using an optical tracking system (NDI co., Spectral), as shown in Fig. 6. To prevent incorrect identification by the optical tracking system due to IR reflections from the metal parts, the robot was temporarily covered with paper during tracking experiment. The angles between links are calculated by (4). The definition and tracking results of the angles are provided in Fig. 7(a) and Fig. 7(b), respectively. In this analysis, the initial offset angle described in Chapter II is also considered as $\theta_{int} = \theta_{offset} = 10.2°$,

$$\theta = \cos^{-1}\left(\frac{v_1\cdot v_2}{\|v_1\|\|v_2\|}\right) = \cos^{-1}\left(\frac{x_1x_2+y_1y_2+z_1z_2}{\sqrt{x_1^2+y_1^2+z_1^2}\sqrt{x_2^2+y_2^2+z_2^2}}\right) \quad (4)$$

As shown in Fig 8(a) and 8(b), the measured results show that the angle difference between Link 1 and the CTM actuator was measured ranging from 0° to 0.65°, and the angle difference of Link 2 was measured ranging from -0.04° to 0.6°. As shown in Fig 8(c), the position error at the RCM point is 0.718mm, which satisfies the require RCM accuracy of 1mm considering the clinical acceptable error and trocar insertion for eye surgery[19, 31, 32].

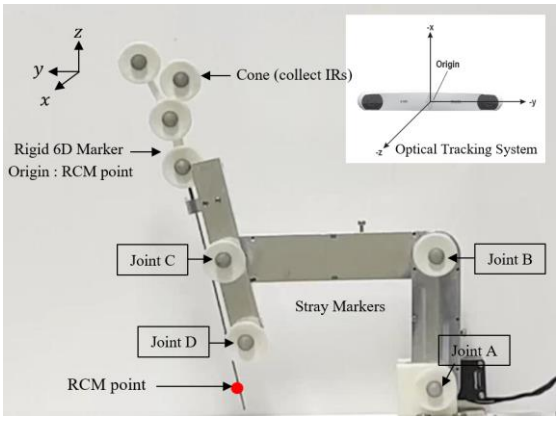

Figure 6. Experimental setup using an optical tracking system.

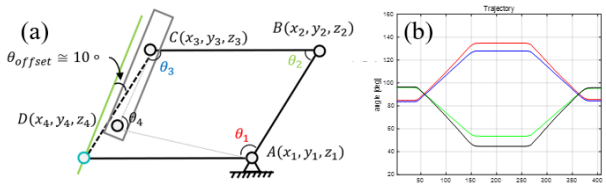

Figure 7. RCM mechanism joint trajectory (a) Joint angle definition, (b) joint trajectory result.

B. Validation of CTM

To validate the CTM's performance, experiments were conducted for tip trajectory tracking and repeatability. Two cameras measured the tip position in the *x*-*y* and *y*-*z* planes, where a pixel-to-real scale was 1 pixel = 0.018 mm for each plane. Using the positions in the two planes, the tip position in 3D space was determined. Initially, the CTM moved along a linear path of 30 mm using the motor values obtained by inverse kinematics. The target accuracy was measured to be 100 μm, but the measured accuracy was 207 μm as shown in Fig 8(d). In teleoperation systems, repeatability is a crucial performance metric, as it allows humans to visually assess and provide feedback. To measure repeatability, the tip's position was measured by approaching five points from all directions in five repeated tests. The experiment results revealed an error of 246 μm as shown in Fig. 8(e).

Possible sources of error include inaccuracies of inverse kinematics, motors' control errors, manufacturing defects, and/or a low measurement resolution. Forward and backward movements exhibited minimal errors (<100 μm), but lateral movements resulted in larger errors due to tube friction.

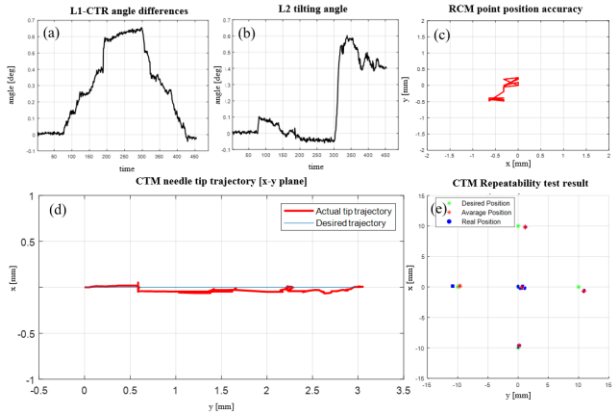

Figure 8. Experiment result (a) (b) RCM joint trajectory, (c) RCM repeatability test, (d) CTM tip trajectory, (e) CTM repeatability test.

C. Targeting Test

The targeting experiment was conducted to assess the reachable workspace to the retina. The experiment was set up as shown in Fig. 9, and an eyeball phantom was created using a 30mm transparent acrylic sphere. In the eyeball phantom, the posterior 2/3 section represents the region corresponding to the retina. Six marked points (A~F) were used to check whether the proposed robot reached each target. The success of targeting was evaluated based on whether the needle tip made contact inside the eyeball phantom at the given points. Results as shown in Fig. 10(a) indicated 100% success in reaching target points when using both CTM and RCM mechanisms.

Comparative experiments were conducted to evaluate the workspace that can reach the retina when using an RCM with a straight needle and an RCM with CTM. In the case of using only the RCM mechanism as shown in Fig 10(b), the needle can reach within the yellow range. But with the CTM+RCM mechanism, the needle tip can reach not only within the range achievable by the RCM mechanism, indicated in the yellow dot, but also within the area marked in red as shown in Fig 10(c). When using a straight needle and CTM, it can reach $x_{RCM} = 64°$ and $x_{CTM} = 220°$. Using the workspace calculation method of (2), the reachable workspaces on the retina were 10.13% and 89.46% of the whole retina, respectively. Another notable point is that the external mechanism needs to move about 32° when using the straight tool and the RCM mechanism, while it moves about 6° when using the CTM+RCM mechanism. This means that 94% less external movement was required when the proposed CTM+RCM robot was used compared to the straight tool. The proposed CTM+RCM robot demonstrated superior reachability compared to the use of a straight needle, covering a larger retina, and it can minimize the external link motion.

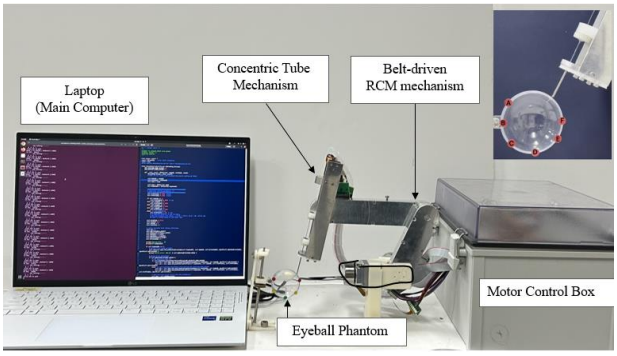

Figure 9. Targeting experiment setup

V. Conclusion

This study presents the design and fabrication of a compact 6-DOF robotic system integrating a compact CTM module and a belt-driven RCM mechanism for vitreoretinal surgery. This robot offers several advantages, including the prevention of tool collisions with the lens, minimal eye damage, and a significantly wider workspace. The proposed mechanism demonstrates the capability to reach 89% of the retina with a tilting motion with roll ±32° and pitch ±85° at the RCM point, ensuring the required workspace both inside and outside of the eyeball.

The experimental results showed an RCM point accuracy of 0.718mm, a CTM position accuracy of 207μm, and a repeatability error of 246μm. Targeting tests revealed that the CRM+RCM mechanism offers a larger reachable retina workspace with minimized external link motion, showing its potential for enhanced eye surgical applications. For future work, we will improve the accuracy and repeatability for the practical eye surgery robot. Since the tele-surgical system can be compensated by human visual feedback, it should improve the control method to enhance repeatability. Additionally, the implementation with force sensing modules or micro grippers is required for practical application. Through these future investigations, we expect that the proposed robotic system will become one of the promising solutions for efficient and minimally invasive eye surgery procedure.

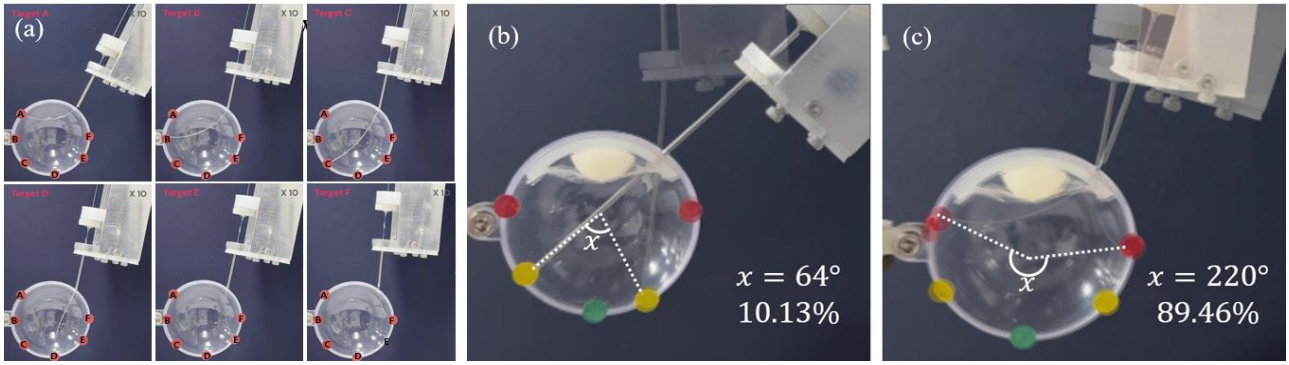

Figure 10. Targeting test result (a) retina targeting result with CTM+RCM mechanism, (b) only the RCM mechanism, (c) with the CTM +RCM mechanism.

REFERENCES

[1] Britannica, The Editors of Encyclopaedia. "retina". *Encyclopedia Britannica*, 1 Dec. 2023, https://www.britannica.com/science/retina. Accessed 20 December 2023.

[2] T. S. Wells, S. Yang, R. A. MacLachlan, J. T. Handa, P. Gehlbach and C. Riviere, "Comparison of Baseline Tremor under Various Microsurgical Conditions," *2013 IEEE International Conference on Systems, Man, and Cybernetics*, Manchester, UK, pp. 1482-1487, 2013.

[3] Z. Elhousseini, E. Lee, T.H.Williamson, "Incidence of lens touch during pars plana vitrectomy and outcomes from subsequent cataract surgery", Retina, 36 (4), pp.825-829, 2016.

[4] B. Davies, "Robotic surgery—a personal view of the past, present and future", Int J Adv Robot Syst, 2015;12:54.

[5] S. Bottger, T. Callar,A. Schweikard, E. Ruckert, "Medical robotics simulation framework for application-specific optimal kinematics", Curr. Dir. Biomed. Eng. 2019, 5, 145–148.

[6] F. -Y. Lin, C. Bergeles and G. -Z. Yang, "Biometry-based concentric tubes robot for vitreoretinal surgery," *2015 37th Annual International Conference of the IEEE Engineering in Medicine and Biology Society (EMBC)*, Milan, Italy, pp. 5280-5284, 2015.

[7] A. Molaei, E. Abedloo, MD. de Smet, S. Safi, M. Khorshidifar, H. Ahmadieh, MA. Khosravi, N. Daftarian , "Toward the art of robotic-assisted vitreoretinal surgery," Journal of Ophthalmic & Vision Research, vol. 12, no. 2, pp. 175–182, 2017.

[8] K. Ikuta, T. Kato and S. Nagata, "Micro active forceps with optical fiber scope for intra-ocular microsurgery," *Proceedings of Ninth International Workshop on Micro Electromechanical Systems*, San Diego, CA, USA, pp. 456-461, 1996.

[9] W. Wei, R. Goldman, N. Simaan, H. Fine, S. Chang. "Design and theoretical evaluation of micro-surgical manipulators for orbital manipulation and intraocular dexterity", In: IEEE international conference on robotics and automation, pp. 3389-3395, 2007.

[10] X. He, V. Van Geirt, P. Gehlbach, R. Taylor, I. Iordachita. "IRIS: integrated robotic intraocular snake", in: IEEE international conference on robotics and automation; pp.1764-1769, 2015.

[11] H.B. Gilbert, D.C. Rucker, R.J. Webster, "Concentric tube robots: the state of the art and future directions", Robot Res. 2016.

[12] M.U.Farooq, B. Xu, and S.Y. Ko, "A concentric tube-based 4-DOF puncturing needle with a novel miniaturized actuation system for vitrectomy", *BioMed Eng OnLine* 18, 46, 2019.

[13] T. da Veiga et al., "Challenges of continuum robots in clinical context: a review", prog.Biomed. Eng. 2, No. 3 032003 , 2020.

[14] J. Wu et al, "An Optimized Tilt Mechanism for a New Steady-Hand Eye Robot," 2020 IEEE/RSJ International Conference on Intelligent Robots and Systems (IROS), pp. 3105-3111, 2020.

[15] M. Jinno and I. Iordachita, "Microgripper Using Flexible Wire Hinge for Robotic Intraocular Snake," *2022 International Conference on Robotics and Automation (ICRA)*, pp. 6218-6224, 2022.

[16] A. Üneri, M. A. Balicki, J. Handa, P. Gehlbach, R. H. Taylor and I. Iordachita, "New steady-hand Eye Robot with micro-force sensing for vitreoretinal surgery," *2010 3rd IEEE RAS & EMBS International Conference on Biomedical Robotics and Biomechatronics*, Japan, pp. 814-819, 2010.

[17] M. Gaafar, M. Magdy, A. T. Elgammal, A. El-Betar and A. M. Saeed, "Development of a New Compliant Remote Center of Motion (RCM) Mechanism for Vitreoretinal Surgery," *2020 6th International Conference on Control, Automation and Robotics (ICCAR)*, Singapore, pp. 183-187, 2020.

[18] A. Mablekos-Alexiou, S. Ourselin, L. Da Cruz, C. Bergeles, "Requirements based design and end-to-end dynamic modeling of a robotic tool for vitreoretinal surgery", in: IEEE international conference on robotics and automation, pp. 135-141, 2020.

[19] N. Wang, X. Zhang, M. Li, H. Zhang, D. Stoyanov and A. Stilli, "A 5-DOFs Robot for Posterior Segment Eye Microsurgery," in *IEEE Robotics and Automation Letters*, vol. 7, no. 4, pp. 10128-10135, Oct. 2022.

[20] E. Rahimy, J. Wilson, TC. Tsao, S. Schwartz, JP. Hubschman, "Robot-assisted intraocular surgery : development of the IRISS and feasibility studies in an animal model, Eye 27, pp,972-978, 2013.

[21] P. E. Dupont, J. Lock, B. Itkowitz and E. Butler, "Design and Control of Concentric-Tube Robots," in *IEEE Transactions on Robotics*, vol. 26, no. 2, pp. 209-225, April 2010.

[22] I. Bekerman, R. Gottlieb, and M. Vaiman, "Variations in Eyeball Diameters of the Healthy Adults", J Ophthalmol, vol. 2014, pp. 1–5, 2014.

[23] L. Wu, B. L. -W. Tan and H. Ren, "Prototype development of a hand-held robotic light pipe for intraocular procedures," *2015 IEEE International Conference on Robotics and Biomimetics (ROBIO)*, Zhuhai, China, pp. 368-373, 2015.

[24] B. Xu, "Development of A Force Measurable Concentric Tube-Based Robotics System for Vitreoretinal Surgery", Ph.D. dissertation, Chonnam National University, 2021.

[25] S. Lim et al, "Robotic Transrectal Ultrasound Guided Prostate Biopsy", IEEE Transactions on Biomedical Engineering, vol. 66, no. 9, pp. 2527-2537, 2019.

[26] W. Yang, "Novel robot structure for a mechanically-scalable motion of intraocular and reconstructive surgery," Ph.D. dissertation, KAIST, 2021.

[27] H.C.M. Meenink, "Vitreo-retinal eye surgery robot: sustainable precision", Ph.D. dissertation,Technische Iniversiteit Eindhoven, 2011.

[28] R. J. Hendrick, S. D. Herrell and R. J. Webster, "A multi-arm hand-held robotic system for transurethral laser Prostate surgery," *2014 IEEE International Conference on Robotics and Automation (ICRA)*, Hong Kong, China, 2014, pp. 2850-2855, 2014.

[29] M. Khadem, L. Da Cruz and C. Bergeles, "Force/Velocity Manipulability Analysis for 3D Continuum Robots," 2018 IEEE/RSJ International Conference on Intelligent Robots and Systems (IROS), Madrid, pp. 4920-4926, 2018.

[30] https://github.com/fsuarez6/phantom_omni.git(Accessed 18 December 2023)

[31] Sakai *et al*., "Design and development of miniature parallel robot for eye surgery," *2014 36th Annual International Conference of the IEEE Engineering in Medicine and Biology Society*, USA, pp. 371-374, 2014.

[32] M. Zhou *et al*., "Towards Robotic-Assisted Subretinal Injection: A Hybrid Parallel–Serial Robot System Design and Preliminary Evaluation," in *IEEE Transactions on Industrial Electronics*, vol. 67, no. 8, pp. 6617-6628, 2020.